Preparation of TiO_2 aerogels by a sol-gel combined solvothermal route†

Zhongqiang Zhao, Xiuling Jiao and Dairong Chen*

Received 6th November 2008, Accepted 24th February 2009
First published as an Advance Article on the web 23rd March 2009
DOI: 10.1039/b819849g

TiO_2 (anatase) aerogels with high surface area were prepared through solvothermally treating the TiO_2 based wet-gels prepared by the sol-gel method, followed by atmosphere-drying to remove the solvents from the gels. This route provided a new strategy for the preparation of crystalline metal oxide aerogels. The microstructure of the aerogel was studied in detail. The aerogels solvothermally treated at 140 °C exhibited a high BET surface area of 528.9 m^2/g. All the aerogels showed extensive photoluminescent emission at 467, 555 and 615 nm, whose intensity decreased with the solvothermal temperature increasing and significantly increased after calcinations.

1. Introduction

As low-density and high surface area nanomaterials, aerogels have potential applications as highly efficient insulation materials, acoustic impedance coupled materials, high-energy particle detectors, drug carriers, catalysts, and catalyst carriers due to their unique porous structures.[1] In recent years, a series of aerogels including metals, organic materials, inorganic compounds, and organic/inorganic hybrid or composite aerogels have been prepared,[2,3] among which silica and carbon aerogels with an amorphous structure have been extensively researched due to their outstanding properties and potential applications in a wide temperature range.[1,4]

The metal compounds such as oxides and sulfides usually exhibit special optical, electrical or magnetic properties only in the crystalline state. Thus many reports focus on the preparation of crystalline aerogels of metal oxides, and two kinds of methods have been developed. The traditional method of producing aerogels is often applied, in which the metal oxide based wet-gel is prepared through hydrolysis-polymerization of metal compound precursors, followed by the supercritical extraction process to remove the solvents from the gel networks with the liquid CO_2, methanol, ethanol, or other solvents as the extractive reagent. In this process, some easily crystallized aerogels such as SnO_2 and ZnO can be obtained,[5] but most metal oxides cannot crystallize at low temperature. In order to prepare their crystalline aerogels, the amorphous aerogels always need high-temperature calcination; however, the frameworks of aerogels are usually destroyed during this process, and low-porous crystalline aggregates are often formed rather than aerogels.[6] In the other recently developed process, the wet-gels are firstly prepared by the nanocrystal surface polymerization reaction, followed by supercritical drying to form crystalline aerogels. This method has been successfully used to prepare II–VI semiconductor aerogels,[3] but the production of crystalline oxide aerogels still remains a challenge due to the complexity of the necessary surface reactions. Thus it is necessary to explore new routes to prepare the crystalline oxide aerogels, particularly those with high crystallization temperatures. Herein, a new strategy to crystalline titanium oxide aerogels is introduced, in which the wet-gels are pre-treated through a solvothermal crystallization reaction and then dried to form aerogels. Comparing to the previous reported TiO_2 aerogels with low crystallinity,[7] the network structure of wet-gels were strengthened through a solvothermal crystallization in the present work, and then dried at atmospheric pressure to yield crystalline TiO_2 aerogels. This new route might be expanded to the preparation of other crystalline oxide aerogels.

2. Experimental section

2.1. Synthesis

All the reagents were analytical grade and were used without further purification.

In a typical synthesis, a mixture of 20.0 mL (0.2713 mol) acetone (CH_3COCH_3, 99%) and 0.54 mL (5.3 mmol) acetylacetone ($CH_3COCH_2COCH_3$, 99%) was added into 6.0 grams (24.07 mmol) of tetrabutyl titanate [$Ti(OC_4H_9\text{-}n)_4$, 99%] under stirring. Then a mixture of acetone (7.6 mL) and water (1.2 mL) was added dropwise to form a sol which gradually transformed into a wet-gel. After aging at room temperature for 24 h, the gel was placed in a 15.0 mL autoclave and acetone was added until 80% of the volume of the autoclave was filled. The autoclave was heated at 120–160 °C to form a crystalline TiO_2 wet-gel, which was then dried at room temperature for 4 h, 50 °C for 4 h, 80 °C for 2 h and 120 °C for 2 h at atmospheric pressure to obtain the crystalline aerogels. The aerogels obtained with the solvothermal temperatures of 120, 140 and 160 °C are respectively named as aerogel-120, aerogel-140 and aerogel-160.

2.2. Characterization

The morphology and structure of the samples were observed *via* transmission electron microscope (TEM, JEM 100CX-II) and high-resolution transmission electron microscope (HR-TEM,

Key Laboratory for Special Functional Aggregate Materials, Education Ministry, School of Chemistry and Chemical Engineering, Shandong University, Jinan 250100, People's Republic of China. E-mail: cdr@sdu.edu.cn; Fax: +86-0531-88364281; Tel: +86-0531-88364280

† Electronic supplementary information (ESI) available: Photographs and HR-TEM images of wet-gels, HR-TEM images of the aerogel obtained from the gel without solvothermal treatment, HR-TEM images and IR spectra of the calcined aerogels, XRD patterns of the aerogels before and after calcination. See DOI: 10.1039/b819849g

GEOL-2010). XRD patterns of the samples were recorded on a Rigaku D/Max 2200PC diffractometer with a graphite monochromator and Cu Kα radiation (λ = 0.15418 nm). Thermogravimetric (TG) analysis was conducted in an air atmosphere at a heating rate of 10.0 °C min^{-1} from 50 °C to 800 °C (TA's SDTQ600 thermal-analyzer). N_2 adsorption- desorption curves of the samples were measured at the temperature of liquid nitrogen (−196 °C), the sample was degassed at 50 °C for 10 h before measurement. BET (Brunauer-Emmett-Teller) and BJH (Barrett-Joyner-Halenda) methods (QuadraSorb SI) were used to give the surface area and the pore size distribution curve. Infrared (IR) spectra of the samples within 400–4000 cm^{-1} were measured on a Nicolet 5DX FT-IR infrared spectrometer using the KBr pellet technique. X-Ray photoelectron spectra (XPS) were recorded on a PHI-5300 ESCA spectrometer (Perkin-Elmer) with its energy analyzer working in the pass energy mode at 35.75 eV, and the Al Kα line was used as the excitation source. Steady state fluorescence spectra were obtained on an Edinburgh FLS920 fluorescence spectrometer equipped with a 450 W Xe lamp and a time-correlated single photon counting (TCSPC) card.

3. Results and discussion

The wet-gels transformed into transparent yellow gels after solvothermal treatment at 120 °C. As the solvothermal temperature increased, the color of the wet-gels gradually became deeper and the brown gels were formed when the temperature reached 160 °C (ESI,† Fig. S1). The monolith gels indicated that the networks of wet-gels were not destroyed during the solvothermal treatment. HR-TEM images (ESI†, Fig. S2) demonstrated that the samples after solvothermal treatment still had interconnected network structures, and the micropores could be observed clearly.

After ambient pressure drying, HR-TEM images (Fig. 1) of the aerogels showed obvious nanopores, indicating their porous structures. The images also showed that the aerogels were composed of nanoparticles with size of several nanometres, and the interface between the particles gradually became clear with solvothermal temperature increasing. The lattice fringes also can be observed clearly, in which the interplanar distances of 0.235 and 0.237 nm with a cross angle of *ca.* 62° can be ascribed to (112) and (004) planes of anatase TiO_2, and those of *ca.* 0.35 nm correspond to (101) planes of anatase TiO_2. The result indicated that the aerogels were composed of anatase TiO_2. In addition, the HR-TEM images confirmed that the crystallinity of aerogels increased as the solvothermal temperature increased. The corresponding XRD patterns also revealed the anatase crystalline nature of the samples (JCPDS, No. 84-1285), and the low intensity of the reflections might relate to the poor crystallinity, the small size of the particles comprising the aerogels as well as the organics in the samples. The crystallinity of the samples increases with the solvothermal temperature increasing, which is consistent with the HR-TEM observation (ESI,† Fig. S6a). The width of the reflections decreases with the intensity of the XRD reflections enhancing, implying the increasing of the TiO_2 nanoparticles composed the aerogels with the solvothermal temperature increasing. As a comparison, the aerogel obtained without solvothermal treatment while other conditions were kept constant showed an amorphous structure (ESI,† Fig. S3), which revealed that the solvothermal treatment of the gels led to the formation of the crystalline anatase titania aerogels.

N_2 adsorption-desorption isotherms (Fig. 2I) of the samples obtained under different conditions showed rapid increase with $P/P_0 < 0.1$ and obvious hysteresis loops in the relative pressure range of 0.4–0.8, indicating the coexistence of micropores and mesopores in the prepared aerogels.[8] The BET surface areas are 447.1, 528.9 and 224.7 m^2/g for the aerogels when the solvothermal temperatures are 120, 140 and 160 °C respectively. The pore size distribution curves (Fig. 2II) indicate that all the aerogels have two kinds of pores with sizes of 1–2 nm (micropore) and 2–5 nm (mesopore), and the mesopores gradually

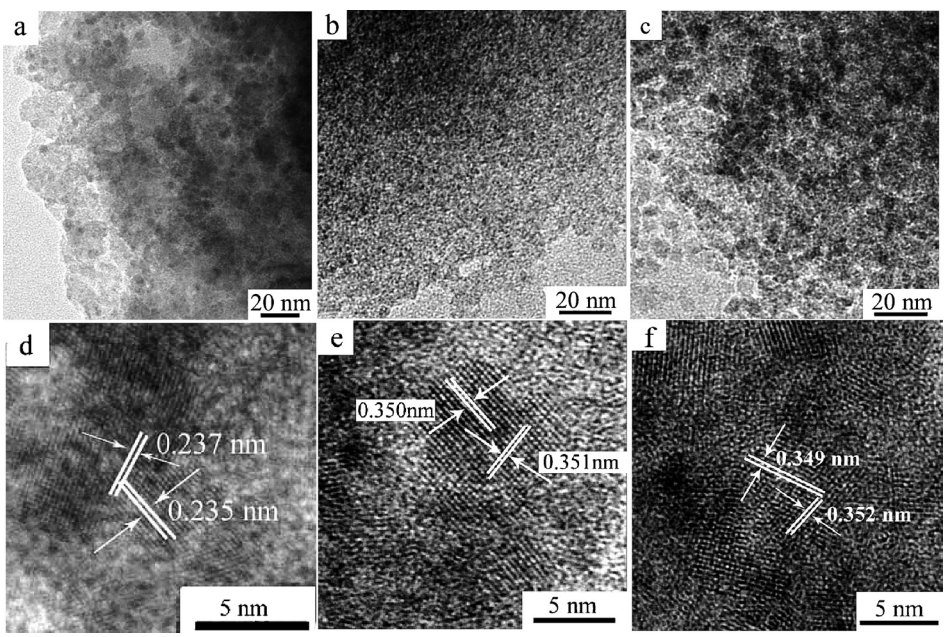

Fig. 1 HR-TEM images of aerogel-120 (a, d), aerogel-140 (b, e), and aerogel-160 (c, f).

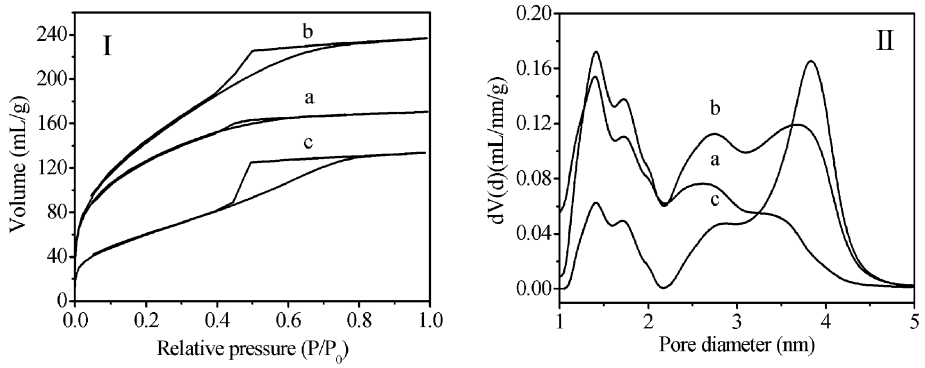

Fig. 2 N_2 adsorption-desorption isotherms (I) and pore size distribution curves (II) of aerogel-120 (a), aerogel-140 (b), and aerogel-160 (c).

increased and the micropores gradually reduced as the solvothermal temperature increased. From 120 °C to 140 °C, the micropores reduced slightly, while the mesopores increased significantly, and the surface area increased significantly. As a comparison, the mesopores slightly increased from 140 °C to 160 °C, and the micropores reduced obviously, resulting in a decrease in surface area.

TGA results (Fig. 3I) showed that the aerogels prepared at different solvothermal temperatures exhibited similar weight-loss temperatures, but the total amount of weight-loss decreased as the solvothermal temperature increased. The first step of weight-loss is within the range 50–160 °C, which is *ca.* 2.0% for all the aerogels and is mainly due to the removal of physically adsorbed organics and water on the surface of nanoparticles comprising the aerogels. The second one from 160 to 270 °C for aerogel-120/-140/-160 is respectively 13.7%, 11.5% and 5.0%, which is mainly attributed to the removal of adsorbed organics and water in the pores. The third step from 270 to 550 °C for aerogel-120/-140/-160 is 16.1%, 15.1% and 7.6% respectively, mainly from the hydroxyls and organics on the particle surface and in the pores. The removal temperature of solvents was higher than their boiling points because of the capillary force of nanopores, as well as the hydrogen bonded interaction between the solvent molecules and Ti–OH. The similar weight-loss temperatures for the aerogels revealed that there were the same kinds of compounds in the aerogels. But the various weight-loss amounts indicated different organic, water and hydroxyl contents in the aerogels, which related to the microstructure such as pore size and density as well as the crystallinity. The TGA results indicated that the volatile substance gradually decreased as the solvothermal temperature increased, implying the decreasing of surface area of

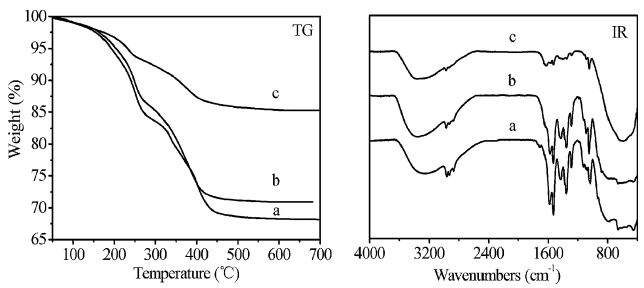

Fig. 3 TG curves and IR spectra of aerogel-120 (a), aerogel-140 (b), and aerogel-160 (c).

the aerogel after solvothermally treated at 160 °C. However, the aerogel-140 exhibited a larger BET surface area than the aerogel-120 although its weight loss is relative small. This indicates that the relatively high crystallinity of aerogel-140 led to a solid network, which was not destroyed during the degassing at 50 °C before N_2 adsorption-desorption measurement.

IR spectra show that the absorptions between 900 cm^{-1} and 3000 cm^{-1} are present at the same positions for all aerogels, but the intensities are different (Fig. 3II). The peaks between 1520 cm^{-1} and 1580 cm^{-1} are attributed to the vibrations of coordinated acetylacetone groups. The absorptions at 2800–3000 cm^{-1}, 1360 cm^{-1}, 1430 cm^{-1} and 1290 cm^{-1} are due to the C–H vibrations, and those at 1000–1200 cm^{-1} are assigned to the C–O vibrations. The bands around 800 cm^{-1} should be assigned to the vibrations of C═O and C–H bonds. The presence of C═O, C–H bonds and acetylacetone groups indicated the existence of organic molecules in aerogels, and the decreasing of the intensities of these absorptions revealed the gradually reducing of the organics in the aerogels with the solvothermal temperature increasing from 140 to 160 °C. In addition to the absorption bands due to the organics, there are broaden absorption bands centered at *ca.* 3400 cm^{-1} and below 800 cm^{-1}. The broad band centered at *ca.* 3400 cm^{-1} is ascribed to the vibrations of O–H bonds, including the hydroxyls from the absorbed water, alcohol and Ti–OH groups. It can be seen that with the solvothermal temperature increasing from 120 to 140 to 160 °C, this band shifts from 3256 to 3356 to 3360 cm^{-1}, indicating different hydroxyls' composition in the aerogels obtained at different solvothermal temperatures. It is known that the existence of hydrogen bonds between the hydroxyls results in the broad IR absorption band and the shift to low wave-number. Combined with the TGA result, it is speculated that the hydrogen bonds between the hydroxyls reduce with the increasing solvothermal temperature. As a comparison, the absorptions below 800 cm^{-1}, which is assigned to the vibrations of Ti–O bonds, show similar characteristics for the aerogels obtained at 120 and 140 °C, while obviously narrow for the aerogel-160. This result indicates that the Ti–OH groups significantly reduced through solvothermal treated at 160 °C, corresponding to the increasing of the crystallinity of the aerogel.[9]

For the aerogel-120/-140/-160, the corresponding XP levels of O1s exhibited at 531.08, 530.71 and 530.02 eV, and the asymmetry morphology of O1s peaks indicated that the oxygen atoms in aerogels should be in more than one state, which might be the

composite peak composed of the crystal-lattice and adsorbed oxygen. The peak-fits (Fig. 4) exhibited a peak corresponding to the crystal-lattice oxygen at 530.33, 530.26 and 529.89 eV and another one corresponding to adsorbed oxygen at 532.40, 532.32 and 532.04 eV, respectively. The crystal-lattice oxygen atoms came from the crystalline TiO_2 framework and the others were due to the surface hydroxyls. From the relative intensities of the two peaks it can be concluded that the lattice oxygen atoms gradually increased as the solvothermal temperature increased, accompanied by the reducing of surface hydroxyls, and this also led to the shift of O1s level.

XP patterns (Fig. 5) showed that the Ti2p3/2 and Ti2p1/2 levels appeared at 458.65, 458.62, 458.42 and 464.41, 464.28, 464.01 eV for aerogel-120/-140/-160, which changed to a higher energy state compared with those of dense anatase TiO_2 in previous report (Ti2p3/2-458.00, Ti2p1/2-464.00 and O1s-529.84 eV). This phenomenon was due to the presence of a large amount of hydroxyls (–OH) on TiO_2 nanoparticles' surface, whose strong polarity and high electro-negativity enhanced the binding energy.[10]

To investigate the thermal stability and microstructure evolution of aerogels, the aerogels were calcined from room temperature to 380 °C with a heating rate of 1.0 °C/min and kept at that temperature for 2 h. The HR-TEM images (Fig. 6) showed that the network of the aerogels still remained which is composed of the well crystallized spherical nanoparticles with the sizes of 7.9, 8.7 and 9.1 nm for aerogel-120/-140/-160 (ESI,† Fig. S4). XRD patterns indicate the crystallinity of the calcined samples obviously increased comparing to the solvothermal aerogels, which is consistent with the HR-TEM observations. The particle sizes calcined based on the Scherrer equation and the breadth of (101) reflections are respectively 8.3, 10.1 and 10.5 nm

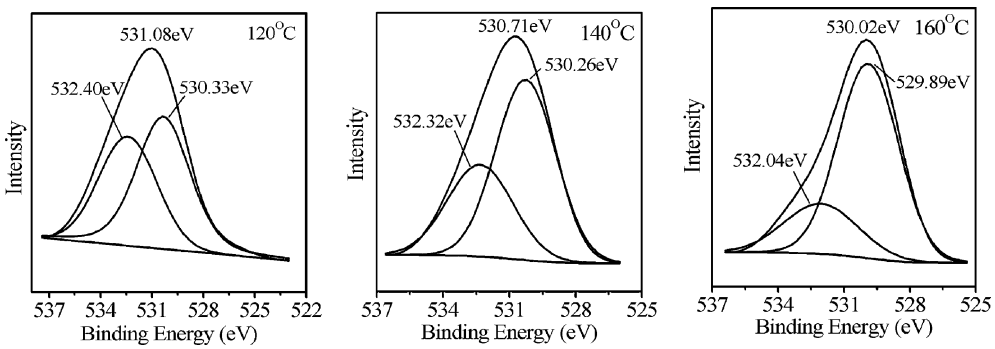

Fig. 4 O1s XP spectra of TiO_2 aerogels solvothermally treated at different temperatures.

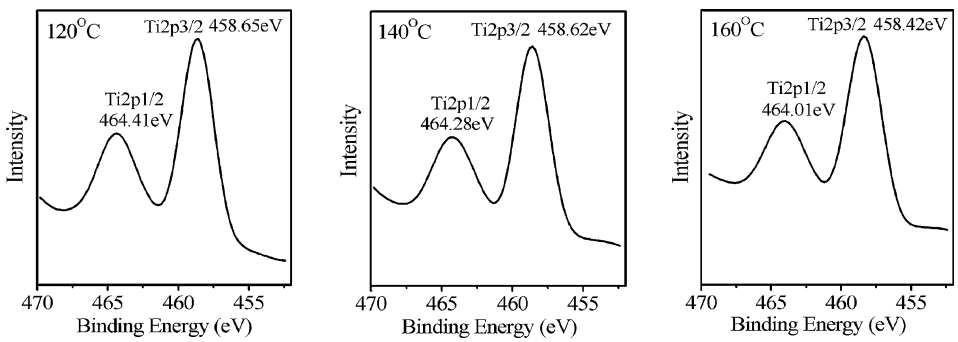

Fig. 5 Ti2p XP patterns of TiO_2 aerogels solvothermally treated at different temperatures.

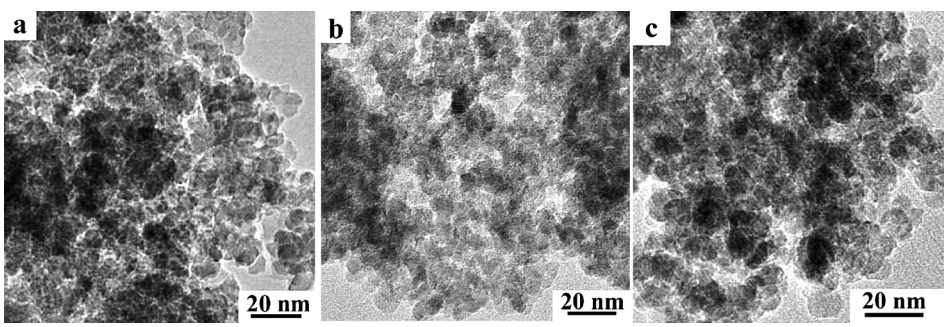

Fig. 6 HR-TEM images of calcined aerogel-120 (a), aerogel-140 (b) and aerogel-160 (c).

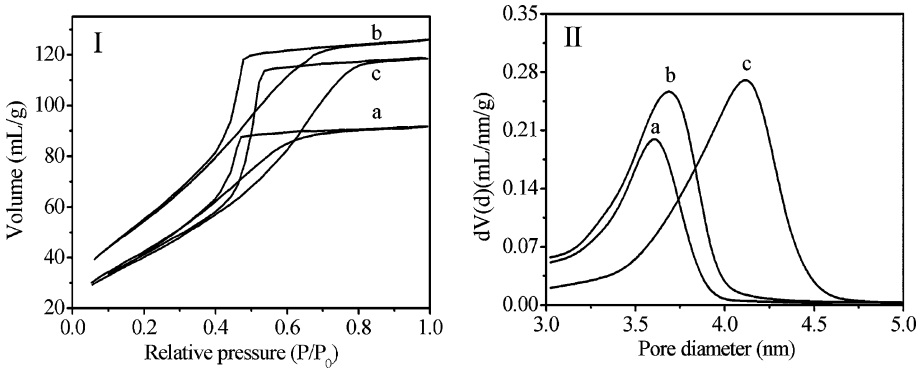

Fig. 7 N_2 adsorption-desorption isotherms (I) and pore size distribution curves (II) of calcined aerogel-120 (a), aerogel-140 (b) and aerogel-160 (c).

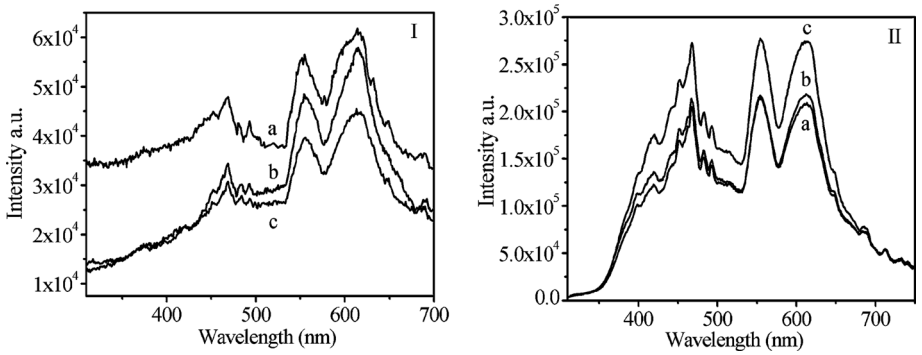

Fig. 8 PL spectra of the as-prepared aerogels (I) and those of calcined aerogels (II). (a) Aerogel-120, (b) aerogel-140, and (c) aerogel-160. The excited wavelength was 260 nm.

for the calcined aerogel-120, 140, 160 (ESI,† Fig. S6). IR spectra showed that the peaks around 2900 cm^{-1} disappeared (Fig. S4†), indicating that the organics in aerogels were decomposed during the calcinations, and those at 1450–1650 cm^{-1} revealed the presence of a few of carbonate groups. N_2 adsorption-desorption curves of calcined aerogels still showed type-IV adsorption isotherms (Fig. 7) with the hysteresis loop, indicating their mesoporous structure nature. For the calcined aerogel-120/-140/-160, the surface areas were 162.3, 209.6 and 151.4 m^2/g, and the average pore sizes were 3.61, 3.77 and 4.16 nm, respectively. Compared with those of aerogels before calcination, the pore size distributions obviously narrowed, in which most of the pores with size of 1–2 nm disappeared and those between 2 and 5 nm remained and expanded to 3–5 nm. The disappearance of small pores and the enlargement of large pores might be due to the removal of –OH groups and organics as well as the growth of TiO_2 nanoparticles during the calcination. As a result, the disappearance of small pores resulted in the decreasing of specific surface area. This indicated that the prepared aerogels had good thermal stability although some small pores disappeared at 380 °C.

Photoluminescence (PL) spectroscopy is a powerful tool for understanding the electronic, optical, and photoelectric properties of materials.[11] It was found that all the aerogels show extensive photoluminescent emission at 467, 555 and 615 nm (Fig. 8I), indicating the similar surface states of the aerogels because the PL emission is mostly a surface phenomenon. According to previous reports,[12] band-gap excitation of TiO_2 in vacuum yields a broad emission between 2.0 and 3.0 eV (415–620 nm), the intensity of which is strongly affected by the presence of electron donor/acceptor molecules. Thus, these emissions are related to the oxygen vacancy such as the single-bridging oxygen vacancy and double-bridging vacancy on the surface as well as other defects. As the solvothermal temperature increased, the intensity of the emissions decreased, which revealed that the defects reduced with increased crystallinity. However, the emissions are significantly enhanced after calcination at 380 °C and the calcined aerogel-160 exhibited relatively intense emission (Fig. 8II), implying a change in the surface state of the samples. The increasing of PL emissions in our experiment might be attributed to the increasing of the surface defects during the annealing of the aerogels,[13] indicating that the number of point defects significantly increased during the calcination without changing the defect types.

4. Conclusions

Titania aerogels with high surface areas were successfully prepared using a solvothermal combined sol-gel method, followed by atmosphere-drying, in which the wet-gels prepared by a sol-gel method which were solvothermally treated at 120–160 °C to yield the crystalline wet-gels (anatase TiO_2). This provides a route to produce crystalline aerogels and might be applied to the preparation of other metal oxide aerogels. The aerogels were transparent monoliths with mesoporous structures and their surface area varied with different solvothermal temperatures. The aerogel derived from the wet-gels after solvothermal

treatment at 140 °C exhibited a maximum surface area of 528.9 m^2/g. After calcination, the surface areas of aerogels would decrease because of the disappearance of small pores. Furthermore, all the TiO_2 aerogels showed peculiar PL emissions, which were enhanced after calcinations.

Acknowledgements

This work was supported by the Program for New Century Excellent Talents in University, People's Republic of China.

References

1 N. Hüsing and U. Schubert, *Angew. Chem., Int. Ed.*, 1998, **37**, 22.
2 A. C. Pierre and G. M. Pajonk, *Chem. Rev.*, 2002, **102**, 4243.
3 (*a*) J. L. Mohanan, I. U. Arachchige and S. L. Brock, *Science*, 2005, **307**, 397; (*b*) I. U. Arachchige and S. L. Brock, *Acc. Chem. Res.*, 2007, **40**, 801.
4 (*a*) F. Detcheverry, E. Kierlik, M. L. Rosinberg and G. Tarjus, *Langmuir*, 2004, **20**, 8006; (*b*) B. E. Yoldas, M. J. Annen and J. Bostaph, *Chem. Mater.*, 2000, **12**, 2475; (*c*) V. Bock, O. Nilsson, J. Blumm and J. Fricke, *J. Non-Cryst. Solids*, 1995, **185**, 233; (*d*) C. Moreno-Castilla and F. J. Maldonado-Hódar, *Carbon*, 2005, **43**, 455; (*e*) J. Lee, J. Kim and T. Hyeon, *Adv. Mater.*, 2006, **18**, 2073.
5 (*a*) T. E. Baumann, S. O. Kucheyev, A. E. Gash and J. H. Satcher Jr., *Adv. Mater.*, 2005, **17**, 1546; (*b*) Y. Gao, C. N. Sisk and L. J. Hope-Weeks, *Chem. Mater.*, 2007, **19**, 6007.
6 (*a*) R. A. Köppel, C. Stöcker and A. Baiker, *J. Catal.*, 1998, **179**, 515; (*b*) D. Suh, T. Park, J. Kim and K. Kim, *J. Non-Cryst. Solids*, 1998, **225**, 168; (*c*) Z. Zhao, D. Chen and X. Jiao, *J. Phys. Chem. C*, 2007, **111**, 18738.
7 (*a*) F. Meng, J. R. Schlup and L. Fan, *Chem. Mater.*, 1997, **9**, 2459; (*b*) S. Kelly, F. H. Pollak and M. Tomkiewicz, *J. Phys. Chem. B*, 1997, **101**, 2730; (*c*) A. R. Howells and M. A. Fox, *J. Phys. Chem. A*, 2003, **107**, 3300.
8 (*a*) A. Fidalgo, J. P. S. Farinha, J. M. G. Martinho, M. E. Rosa and L. M. Ilharco, *Chem. Mater.*, 2007, **19**, 2603; (*b*) S. Mulik, C. Sotiriou-Leventis and N. Leventis, *Chem. Mater.*, 2007, **19**, 6138; (*c*) P. P. E. A. de Moor, T. P. M. Beelen and R. A. van Santen, *J. Phys. Chem. B*, 1999, **103**, 1639; (*d*) L. Tosheva and V. P. Valtchev, *Chem. Mater.*, 2005, **17**, 2494.
9 (*a*) D. Chen and X. Jiao, *J. Am. Ceram. Soc.*, 2000, **83**, 2637; (*b*) D. Chen and R. Xu, *J. Mater. Chem.*, 1998, **8**, 965.
10 (*a*) N. Sakai, R. Wang, A. Fujishima, T. Watanabe and K. Hashimoto, *Langmuir*, 1998, **14**, 5918; (*b*) T. Horikawa, M. Katoh and T. Tomida, *Micro. Meso. Mater.*, 2008, **110**, 397; (*c*) C. Wang and S. Ro, *Mater. Chem. Phys.*, 2007, **101**, 41; (*d*) J. Premkumar, *Chem. Mater.*, 2005, **17**, 944.
11 H. Xin, Y. Ebina, R. Ma, K. Takada and T. Sasaki, *J. Phys. Chem. B*, 2006, **110**, 9863.
12 N. Serpone, D. Lawless and R. Khairutdinovt, *J. Phys. Chem.*, 1995, **99**, 16646.
13 G. Lu, A. Linsebigler and J. T. Yates Jr., *J. Phys. Chem.*, 1994, **98**, 11733.